Plasma boundary shape control and real-time equilibrium reconstruction on NSTX-U

M. D. Boyer[1], D. J. Battaglia[1], D. Mueller[1], N. Eidietis[2], K. Erickson[1], J. Ferron[2], D. A. Gates[1], S. Gerhardt[1], R. Johnson[2], E. Kolemen[3], J. Menard[1], C. E. Myers[1], S. A. Sabbagh[4], F. Scotti[5], P. Vail[3]

[1]Princeton Plasma Physics Laboratory, Princeton, New Jersey, USA
[2]General Atomics, San Diego, California, USA
[3]Department of Mechanical and Aerospace Engineering, Princeton University, Princeton, New Jersey, USA
[4]Department of Applied Physics and Applied Mathematics, Columbia University, New York, New York, USA
[5]Lawrence Livermore National Laboratory, Livermore, CA, USA

E-mail: mboyer@pppl.gov

July 2017

Abstract. The upgrade to the National Spherical Torus eXperiment (NSTX-U) included two main improvements: a larger center-stack, enabling higher toroidal field and longer pulse duration, and the addition of three new tangentially aimed neutral beam sources, which increase available heating and current drive, and allow for flexibility in shaping power, torque, current, and particle deposition profiles. To best use these new capabilities and meet the high-performance operational goals of NSTX-U, major upgrades to the Plasma Control System (PCS) hardware and software have been made. Several control algorithms, including those used for real-time equilibrium reconstruction and shape control, have been upgraded to improve and extend plasma control capabilities. As part of the commissioning phase of first plasma operations, the shape controller was tuned to control the boundary in both inner-wall limited and diverted discharges. It has been used to accurately track operator shape evolution requests and produce repeatable discharge evolutions, contributing to achieving $I_p = 1$MA, $B_T = 0.65$T scenarios on NSTX-U, as well as discharges with 2s pulse length.

1. Introduction

The National Spherical Torus eXperiment Upgrade facility (NSTX-U) [1], which completed its first plasma operation campaign in 2016 [2, 3, 4], aims to span between the previous class of spherical torus devices, like NSTX [5] or the Mega-Ampere Spherical Tokamak (MAST) [6], and future facilities planned to study plasma-material interaction [7], nuclear components [8], and demonstration of fusion power production

[9, 10]. NSTX-U looks to build upon the results of NSTX [11] to improve the physics understanding of several key issues for future devices, including the scaling of electron transport with field and current [12, 13, 14, 15], the physics of fast particles [16, 17, 18, 19], and the achievement and sustainment of non-inductive, high-β scenarios [20, 21, 22, 23, 24, 25]. One of the primary components of the upgrade project was the replacement of the 'center stack' (containing the inner-leg of the toroidal field (TF) coils, the Ohmic heating (OH) solenoid, and some divertor coils) with one capable of reaching much higher fields and providing more Ohmic flux for longer discharges. The second major upgrade was the addition of a second neutral beam injector, aimed more tangentially, which significantly increases the auxiliary heating power and neutral beam current drive, and adds flexibility in shaping the spatial deposition of these quantities in the plasma. The upgrade will increase the TF capability from 0.55T to 1.0T, the maximum plasma current from 1.3 MA to 2.0 MA, and enable full-field discharge durations of 5s.

In order to achieve the research goals of the NSTX-U program, real-time protection and control capabilities beyond those demonstrated on NSTX will be required. The NSTX-U Control System (NCS) (which includes the real-time hardware, protection systems, and software) includes the flexible Plasma Control System (PCS) software platform provided by General Atomics [26, 27] that allows customized categories of various control algorithms to be developed within a powerful real-time control infrastructure. As part of the upgrade, many improvements to the NCS hardware have been made to increase the computational power available for the PCS, reduce latency, and expand the number of diagnostics and actuators under real-time control [28]. A significant amount of software development was completed during the upgrade to create the new control algorithms needed to optimally handle the complex dynamics of the system. Ongoing development (e.g., [29, 30, 31, 32]) aims to enable current and rotation profile control, as well as power and particle exhaust control, building on the successful advances in control made during NSTX operations [33, 34, 35, 36].

One of the first commissioning activities during plasma operations was the establishment of reliable feedback control of the plasma position and the shape of the plasma boundary. Early in plasma operations, a gap control algorithm based on only a few of the available sensors and coils was commissioned. This algorithm is still in use during the start-up and ramp-down phase of discharges. Once the plasma current is high enough that reliable real-time equilibrium reconstructions can be completed, a controller based on reconstructed equilibria is activated. This shape controller has been tuned to control both inner-wall limited and diverted discharges and has been used to control the X-point and strike-point positions, as well as the vertical bias of the discharge. A new algorithm for controlling the plasma inner gap, which is a challenge on spherical torus devices, has also been commissioned. The shape control system has enabled accurate boundary control and repeatable discharge evolutions, which has thus far contributed to achieving scenarios on NSTX-U of up to 1MA, 0.65T, and discharges with a 2s pulse length [2, 3], as well as high beta discharges calculated to be over the no-wall stability

limit [37].

1.1. Organization

The paper is organized as follows. In Section 2, the gap control method used during the start-up and shutdown phases of discharges is described. Modifications to the real-time reconstruction code are described in Section 3. In Section 4, updates to the isoflux shape algorithm are described and results of controlling the outer gaps, X-point locations, strike point locations, vertical bias, and inner gap are presented. Conclusions and future work are discussed in Section 5.

2. Coil current and boundary gap control

The gap control algorithm in the PCS controls the poloidal-field (PF) coil voltages to either track a coil current target or to control the plasma outer gap and elongation based on a estimates of these quantities from a small set of flux loop and field measurements. The latter capability is intended to control the plasma position during the early and end parts of discharges when the plasma current is not large enough for reliable real-time equilibrium reconstruction. While a similar gap control approach was used on NSTX, the new version has been updated to include feedback control of the plasma elongation through the PF3 coils, which were only used in feedforward "current control" mode on NSTX. This is an important new feature for maintaining good control of the plasma shape when ramping up using different initial Ohmic coil currents or when switching into the algorithm during plasma ramp-down. For those coils selected to be under "current control", the target current is calculated as

$$I_{target} = C_{PF} I_{P,LP} + f_{PF} I_{OH,LP} + I_{PF,offset} \tag{1}$$

where C_{PF} is a proportionality constant to the low-pass filtered measurement of the plasma current $I_{P,LP}$, f_{PF} is a proportionality constant to the low-pass measurement of the Ohmic coil current, and $I_{PF,offset}$ is the operator programmed current target offset. The proportionality constants are used, for example, to maintain approximately fixed X-point positions by scaling the divertor coil currents with the plasma current, or to reject the effects of the Ohmic coil fringing field. Appropriate values of C_{PF} and f_{PF} were determined by scanning a target range of I_{OH}, I_P, β_N, l_i, κ, and other shaping parameters in a free boundary equilibrium code. A proportional-integral-derivative (PID) controller is used to modify the voltage requests for each coil to track its target current.

For those coils that are configured for use in the gap control algorithm (PF3U/L and PF5) their voltage request is determined based on flux errors. A flux error for the outer gap, $E_{gap,out}$ is calculated as

$$E_{gap,out} = \psi_{outp} - \psi_{in} - (\frac{\partial \psi_{outp}}{\partial R} \cdot g_{out}), \tag{2}$$

where ψ_{in} is an inboard flux measurement, ψ_{outp} is an outboard flux measurement, $\frac{\partial \psi_{outp}}{\partial R}$ is the radial gradient of the outboard flux measurement, and g_{out} is the desired gap between the outboard flux measurement and the plasma edge. The inboard flux measurement is provided by a single flux loop circling the center stack near the mid-plane. ψ_{outp} is formed by weighting the flux measurements from pairs of up-down symmetric flux loops on the primary passive plates, i.e.,

$$\psi_{outp} = \sum_{i=1}^{3} \left[\beta_i \left(\psi_{PPPU,i} + \psi_{PPPL,i}\right)/2\right] / \sum_{i=1}^{3} \beta_i, \tag{3}$$

where β_i is the weight on the i-th flux loop pair. Its radial derivative is calculated using up-down symmetric Mirnov coils positioned close to each flux loop:

$$\frac{\partial \psi_{outp}}{\partial R} = \sum_{i=1}^{3} \left[\beta_i \pi R_{sensor,i} \left(B_{PPPU,i} + B_{PPPL,i}\right)/2\right] / \sum_{i=1}^{3} \beta_i. \tag{4}$$

The Mirnov coils measure both radial and vertical components of the magnetic field, thus equation 4 assumes the poloidal field is up-down symmetric such that the sum of the sensor signals isolates the vertical component of the field. A second flux error, $E_{gap,sp}$ is calculated as

$$E_{gap,sp} = \psi_{outp} - \psi_{outs} - \left(\frac{\partial \psi_{outp}}{\partial R} g_{sp}\right). \tag{5}$$

ψ_{outs} is formed by weighting the flux measurements from pairs of up-down symmetric flux loops on the secondary passive plates, i.e.,

$$\psi_{outs} = \sum_{i=1}^{3} \left[\epsilon_i \left(\psi_{SPPU,i} + \psi_{SPPL,i}\right)/2\right] / \sum_{i=1}^{3} \epsilon_i. \tag{6}$$

This flux difference is used as a proxy for the curvature of the flux surfaces around the passive plates. A more positive value makes the flux surfaces more elongated. The flux errors are then converted to coil current errors using the gain matrix M_G, i.e.,

$$\begin{bmatrix} E_{PF5} \\ E_{PF3} \end{bmatrix} = M_G \begin{bmatrix} E_{gap,out} \\ E_{gap,sp} \end{bmatrix}. \tag{7}$$

Finally, a PID control algorithm is used to adjust the voltage requests for each coil to drive this calculated current error to zero.

An example of the performance of this algorithm for a diverted L-mode discharge with 1MW NBI heating produced early in NSTX-U operations prior to commissioning real-time equilibrium reconstruction based shape control is shown in Figure 1. In this shot, PF1A was the only divertor coil pair used, and was controlled using the relational scheme from (1).The inboard and secondary flux surfaces (dashed-lines), along with the plasma boundary (solid lines) are shown in Figure 1(a) for $t = 0.4$s (start-of-flattop) and $t = 1.0$s (end-of-flattop). The average radial positions of intersections of the the inboard and secondary flux surfaces with the control segments are effectively the controlled quantities. Time traces of these quantities are shown in Figure 1(b), showing that after

some small oscillations during the ramp-up phase of the discharge, the controller is able to hold the inboard and secondary flux surfaces relatively fixed throughout the flattop. A steady-state error between the requested and real-time calculated values persists due to the use of only proportional gain in this discharge. Also shown are the post-shot, fully-converged, magnetics-only EFIT (EFIT01) calculated flux surface locations, showing that while the secondary flux location is well-estimated by the real-time algorithm, the inboard flux position is offset from the EFIT01 calculated position. The main driver of the difference in EFIT01 and the position calculated by equation 4 is the assumption that the radial derivative of the flux is a constant along the control segment. Since the shot is diverted, the inboard flux surface position is offset from the plasma boundary location. The controller is able to achieve acceptable time response and keep these quantities steady throughout the flattop discharge. The offsets between actual and estimated flux surface positions are acceptable for the early and late parts of the discharge where the desired shape evolution is independent of the experiment, or for controlling highly-reproducible discharges, as the operator can empirically achieve desired outer gap sizes and elongations by adjusting the requested values from shot-to-shot during scenario development activities. However, the wide range of proposed scenarios on NSTX-U requires more sophisticated shape control.

3. Real-time equilibrium reconstruction

To enable more precise control of the plasma shape during the main part of the discharge, a realistic solution to the plasma force balance is calculated in real-time, providing a better estimation of the position of the plasma boundary. The rtEFIT algorithm [38] was used for real-time equilibrium reconstruction for several years on NSTX, beginning in 2003 [33]. For NSTX-U, several updates and upgrades have been made to the algorithm. First, the coil and vessel model used in the reconstruction was updated (new tables of Green's function values were calculated) to reflect the new center-stack and other changes made to the device during the upgrade. The number of magnetic diagnostics on the machine was increased during the upgrade, and a majority of the new and existing measurements were made available to the real-time system [39]. The finite elements of the vessel model were combined into thirty groups of elements, each associated with a loop voltage measurement, and the optimal 'effective resistances' were identified for each group based on vacuum magnetic diagnostic calibration shots for use in the measurement of vessel eddy currents in real-time as described in [40]. The spatial grid used to discretize the model of the plasma current was increased from 33x33 to 65x65, now matching the resolution of the standard offline EFIT code used for NSTX-U [41, 42]. This increase in resolution reduces the uncertainty in the computed plasma boundary, especially the X-point locations. To keep the real-time reconstructions as close to the offline reconstructions as possible, the plasma current model parameterization was chosen to match that of the offline code as well.

The rtEFIT algorithm is split into a 'slow loop', which completes an iteration

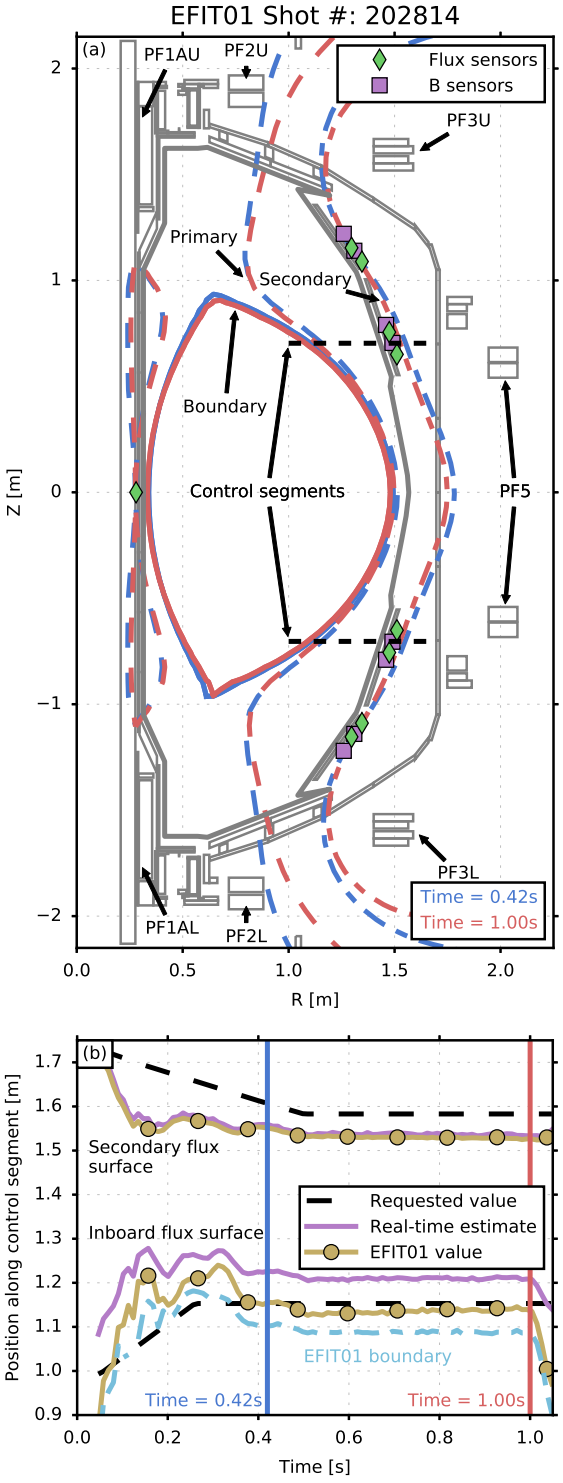

Figure 1. (a) Comparison of plasma boundaries (solid), inboard flux surfaces (dashed), and secondary flux surfaces (dash-dot) at t=0.42s and t=1.00s during shot 202814, along with the flux sensors (green diamonds) used in the online calculation of intersections with control segments (black-dashed). (b) Time traces of the position along the control segments of the requested (black, dashed), online estimated (purple, solid), and offline EFIT01 estimated (gold, circles) inboard and secondary flux surfaces, along with the EFIT01 estimated plasma boundary (light blue, dash-dot).

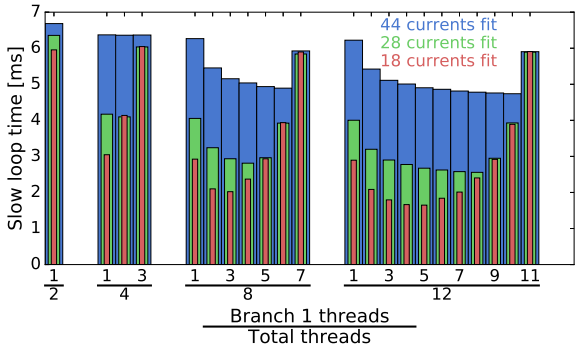

Figure 2. Slow loop time as a function of thread distribution and number of vessel currents fit.

of the equilibrium reconstruction, and a 'fast loop' which updates the errors used by the shape controller on a 200μs time scale based on the response matrix calculated in the last completed slow loop and the latest measurements (see [38] for details). PCS hardware and software improvements (including upgrading the computing infrastructure to use 64 2.8 GHz cores and upgrading compiler tools to take advantage of the newer hardware) enabled completion of the rtEFIT slow loop calculations with vessel current measurements treated as known values (zero uncertainty in fitting) at the new increased grid resolution to be as low as 3.4ms. However, timing tests using processor-in-the-loop (PIL) simulations of the control system showed that the calculation time became unacceptably slow when treating the vessel currents as uncertain fitted parameters and calculating β_N, ℓ_i, and the q profile in real-time. To overcome this limitation, the system was set up to make use of the multi-threading capabilities of rtEFIT and the remaining available cores on the real-time computer. In this mode, the rtEFIT calculations are split into three branches: a set of serialized data processing tasks (branch 0), and two independent branches (branch 1 for the equilibrium reconstruction and branch 2 for the calculation of β_N, ℓ_i, and the q profile) that can be run in parallel after completing the branch 0 tasks. Through the PCS user interace, the total number of threads allocated for rtEFIT, all of which are used for the branch 0 tasks, can be distributed to the parallel branches. A PIL simulation study was performed to assess the timing benefits of increasing the total number of threads and to optimize the allocation of threads between the two branches. The results, displayed in Figure 2, show that using 10 branch 1 threads and 2 branch 2 threads enables fitting 44 currents with a slow loop time $<$5ms. As the number of fitted currents is reduced, the optimal mix of threads shifts, favoring more branch 2 threads, and the slow loop time drops below 2ms. The optimal time drops as the total number of threads increases, however the drop is less significant for larger numbers of fitted currents, indicating that improvements to the parallelization of the fitting procedure may be needed to keep the slow loop time small compared to the characteristic time of the vessel, which is around 10ms. A comparison of the reconstructed distance along the control segments used for shape control (described

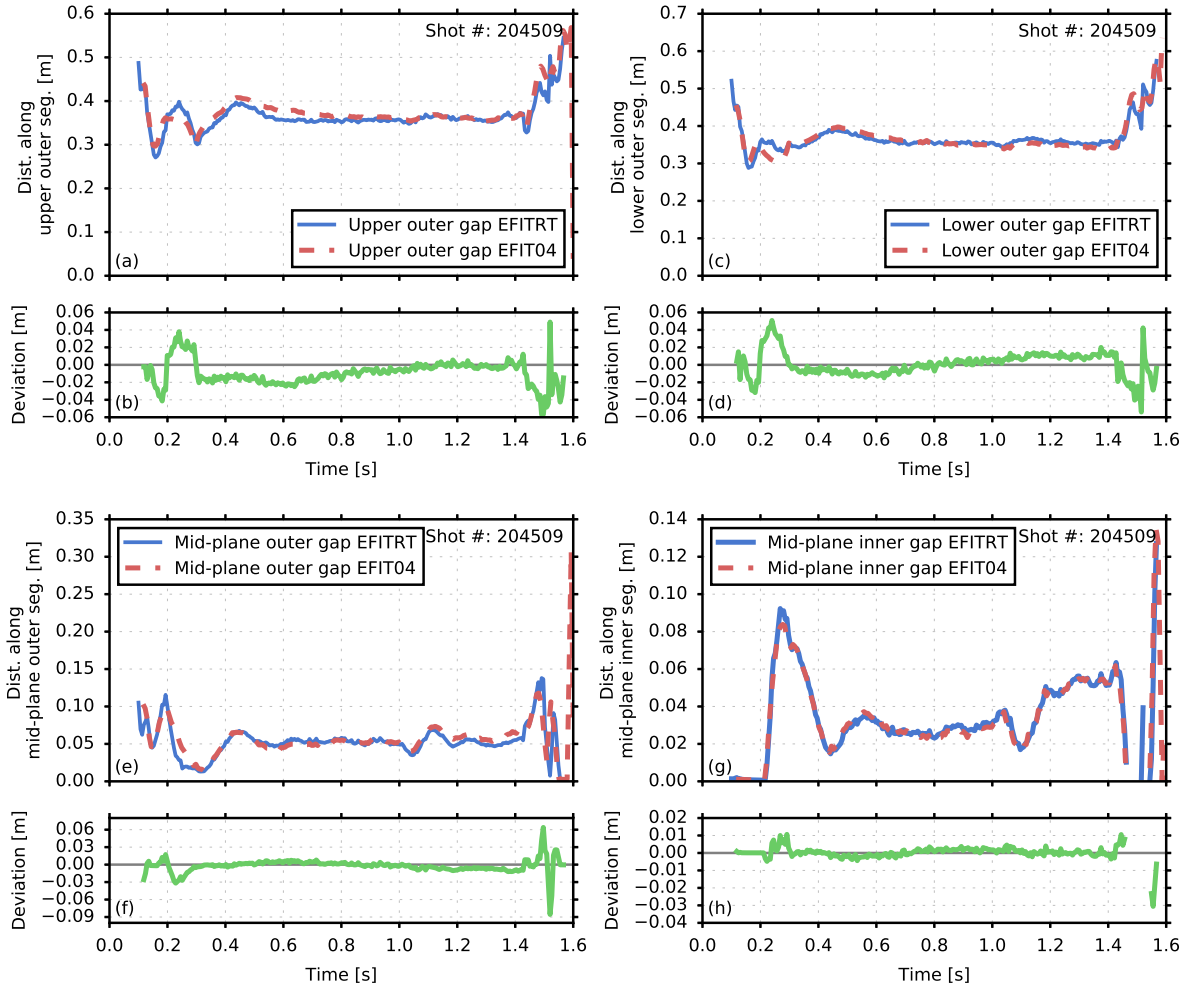

Figure 3. Comparison of the reconstructed distance along the control segments used for shape control for real-time EFIT, EFITRT (blue, solid), and off-line magnetics-only fully converged EFIT, EFIT04 (red, dashed), along with the deviation between the two reconstructions (green, solid).

in the following section) resulting from the real-time EFIT (EFITRT) calculations with all vessel currents fit and an off-line magnetics-only fully converged EFIT (EFIT04‡) is shown in Figure 3. Very similar results are obtained for all four segments, with the largest errors occurring during transients during plasma current ramp-up ($t < 0.4s$)and ramp-down ($t > 1.42s$). During flattop, the deviation remains below 2cm. Future software and hardware upgrades will aim to achieve faster slow loop computation time to enable multiple iterations per slow loop cycle while still fitting vessel currents, which should reduce discrepancies. Optimization of the discretization of the vessel model (to reduce the number of fitted currents while maintaining fidelity) will also be explored.

While the measured signals entering the real-time system are sampled with a 200μs

‡ The automatic post-shot fully converged magnetics-only EFIT run is referred to as EFIT01. EFIT04 is used for special runs, in this case activating the option to include a rigid vertical shift of the plasma in the fit. This option is not typically used in EFIT01 but its use is enforced in real-time EFIT.

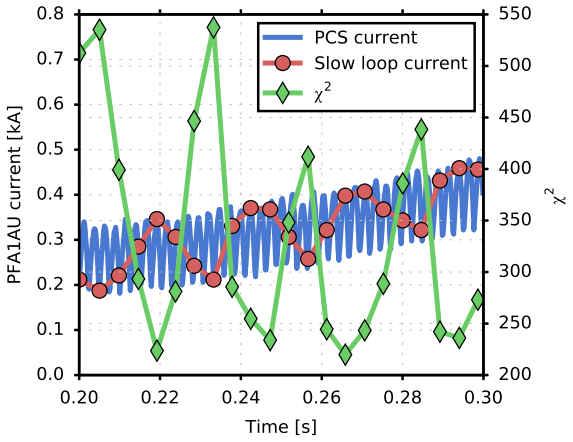

Figure 4. Low frequency oscillations in measurement fitting error χ^2 (red, diamond markers) clearly correlated with the low frequency oscillations of samples at the slow loop cycle times (black, circle markers) of the measured PF1AU coil current (blue, solid).

data acquisition rate, the slow loop of rtEFIT runs at a reduced sample time and is therefore subject to corruption by under sampling high-frequency signals. On NSTX this effect did not cause problems with the reconstructions, however, it was observed on NSTX-U that the high frequency current ripple caused by the rectifiers for the the new lower-inductance PF1A coils was aliased into low frequency oscillations in the reconstruction. This aliasing effect, which is illustrated in Figure 4, had only a small effect on the boundary reconstruction, however, it caused significant errors in the fit to the magnetic measurements and large oscillations in global quantities like β_N and l_i. Since future feedback control algorithms will make use of these calculated signals, it is important to improve the quality of their estimation. To resolve the problem, a digital implementation of a multi-pole filter running on the fast (200μs) sample rate was added to filter the measurements prior to their being sent to the CPU that does the slow loop calculation. A 2nd-order Butterworth filter with its cutoff frequency equal to half of the slow loop sampling frequency was found to effectively remove the oscillations due to aliasing and improve the overall fit to the magnetic measurements. The improvement in fitting and estimation of β_N on data from discharge 204200 is shown in Figure 5. It is also planned to reduce the magnitude of the current ripple in future campaigns with the addition of series inductors to the divertor coil circuits.

4. Isoflux shape control

Based on the real-time equilibrium reconstructions calculated by rtEFIT, the NSTX control system used the isoflux control [43, 38] approach to track the operator requested plasma boundary shape evolution [33]. In this approach, the flux at a set of target locations, referred to as control points and defined by the intersection of the operator

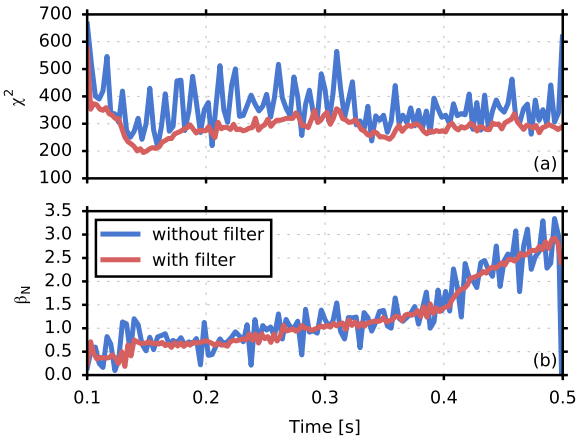

Figure 5. Comparison of the diagnostic fitting error (top) and the calculated value of β_N (bottom) for discharge 204200 with the anti-aliasing filter off (red, circular markers) and the anti-aliasing filter on (blue, solid).

programmed target boundary shape with a set of control segments, is controlled to match a reference flux through feedback modification of the voltage applied to the poloidal field coils. Depending on the plasma configuration, the reference flux may be defined by the flux at a limiter touch point or an X-point. Figure 6 shows the control segments, grids, and points for a typical diverted discharge, along with the coils used for active control during initial NSTX-U plasma operations. The vector of flux errors and the errors between the reconstructed and target X-point locations are each operated on by PID controllers, resulting in a vector P, which is then multiplied by the mixing matrix M, chosen to scale and distribute the P vector values to the appropriate coils in the form of power supply voltage requests. For the results described in this section, the M matrix and PID gains were initially tuned in simulations using a a vacuum coil/vessel circuit model, i.e., only considering the dynamic response of flux to changes in coil and vessel currents, not changes due to the plasma. Gains were then fine tuned empirically during a small number of commissioning discharges to achieve the desired time response. On NSTX, separate feedback algorithms were used to control inner-wall limited discharges and diverted discharges, with the latter enabling control of X-point and strike point locations [35, 36]. For NSTX-U, the code for both algorithms has been re-written to make use of the code generator capability included in the General Atomics supplied PCS software package [28], improving maintainability and making future upgrades easier to implement. For example, the number of lines of code specific to the diverted plasma control algorithm was reduced by 75% while maintaining all original capabilities and adding several new ones.

4.1. Control of inner-wall limited shapes

The inner-wall limited algorithm, which adjusts the coil voltage requests to match the flux at the control points to the flux at the center-stack touch point, has been

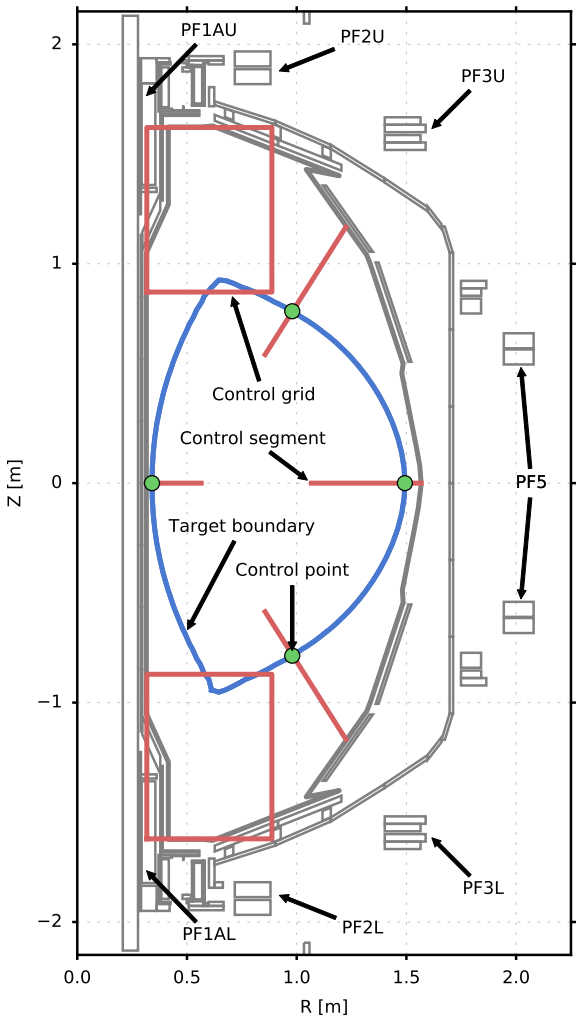

Figure 6. Control segments and grids used in the isoflux algorithms, showing the control points that are controlled during a typical diverted L-mode discharge.

commissioned to use the PF3 upper and lower coils and the PF5 coils to control three points on the outer boundary of the plasma. In Figure 7, the distances from the start of the control segment to the target and achieved boundary intersection point are compared for both the mid-plane outer gap and the lower outer gap for discharge 203474. The results show that after some initial small oscillation, the boundary intersections remain very close to the the target locations (within 2-3cm) throughout the discharge, slowly getting closer over time due to the integral term in the controller. The upper outer gap is not displayed because it has an identical target and nearly identical evolution during the discharge.

4.2. Control of diverted shapes

To transition to a diverted discharge, the divertor coils are controlled to track a pre-programmed current trajectory to bring X-points into the vessel. Once the plasma is

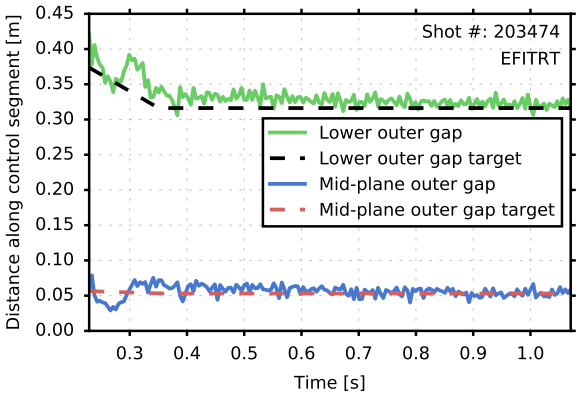

Figure 7. Tracking performance during a limited discharge showing the target (magenta, square markers) and achieved (black, solid) mid-plane outer gap, as well as the target (red, diamond markers) and achieved (blue, solid) lower outer gap for discharge 203474.

brought close to forming an inner gap, the operator programs a transition to the diverted discharge algorithm. In the previous version of the diverted discharge algorithm, the PF3 coils and PF5 coils were used to control the flux at three points on the outer boundary of the plasma to match the flux at the dominant X-point. The algorithm has been modified to automatically switch to use the center-stack touch point as its reference point if the plasma is still limited when the operator programmed algorithm transition occurs, or if the plasma happens to limit during the shot. Prior to this modification, if the plasma happened to limit on the center-stack due to a disturbance or oscillation while using the diverted discharge isoflux algorithm, the controller still used the dominant X-point flux as its reference flux, which was no longer equivalent to the flux at the plasma boundary. This discrepancy in the reference flux resulted in the plasma boundary being pushed inboard, often causing the plasma to stay in a limited configuration throughout the remainder of the shot with the dominant X-point flux surface, instead of the actual plasma boundary, passing through the control points. This is illustrated in 8 (a). In shots with the modification to the selection of the active reference flux, like the one shown in Figure 8(b), the boundary is controlled to pass through the control points as desired, even if the plasma happens to momentarily limit during an oscillation.

4.3. Control of X-point and strike point locations

The PF1AU/L and PF2U/L coils have been commissioned to simultaneously control either the X-point radial and vertical positions or the X-point heights and the radius of the outer strike points. While the previous (NSTX) X-point and strike point control scheme linked each quantity to a single coil [36], the X-point and strike point control for NSTX-U is multi-input-multi-output (MIMO), accounting for the interaction of the coils in the control law. The MIMO control law was obtained by calculating the Jacobian matrix relating changes in coil currents to changes in X-point and strike

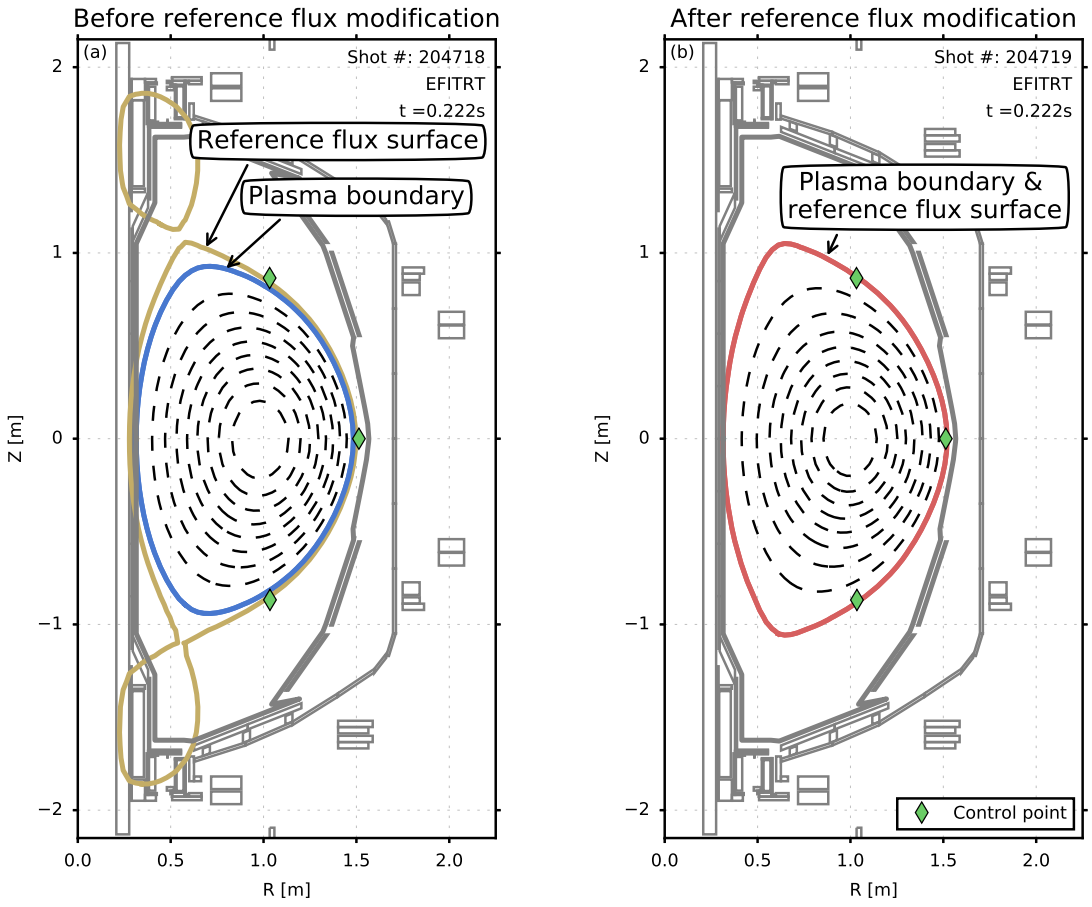

Figure 8. (a) Plasma boundary (blue), the flux surface defined by the dominant X-point flux (gold), and the outer gap control points at 0.22s in discharge 204718, in which the reference flux modification had not yet been implemented. (b) Plasma boundary (red) and outer gap control points at 0.215s in discharge 204719, which had the reference flux modification active.

point locations for a particular target equilibrium, and finding the weighted pseudo-inverse of this matrix. Weights were chosen according to which quantities were to be controlled for a particular shot (the combinations of X-point radial and vertical position as well as X-point vertical position and outer strike point radial position were considered during this campaign). The pseudo-inverse matrix, which indicates the optimal 'direction' for changing coil currents in response to X-point location and strike point flux errors, was entered into the appropriate elements of the isoflux algorithm's M matrix, while PID gains for the respective error quantities were chosen, as described before, based on simulations of the coil/vessel circuit model and fine tuned empirically during commissioning discharges. In Figure 9, successful tracking of the X-point radial and vertical position during the diverted discharge 204602 is shown.

Use of the feedback controller to track series of step changes in the requested outer strike point positions during a single shot (203879) is illustrated in Figure 10. The controller was able to track the requests at each step, while keeping the X-point heights

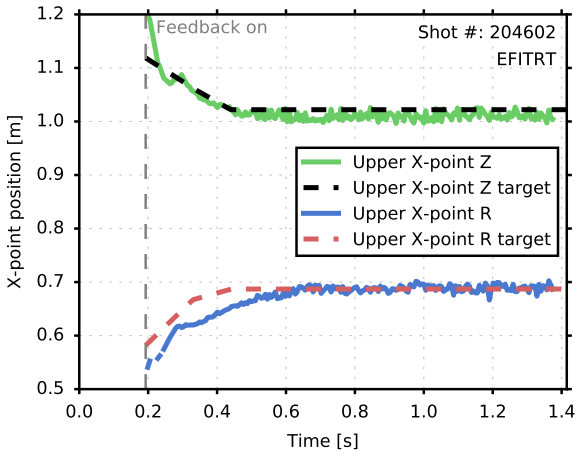

Figure 9. X-point position tracking performance during a diverted discharge showing the target (black, dashed) and achieved (green, solid) upper X-point Z position, as well as the target (red, dashed) and achieved (blue, solid) upper X-point R position for discharge 204602.

and the outer boundary locations fixed. Carbon II emission on the lower divertor during the shot is shown in Figure 11, along with the target and reconstructed strike-point positions. The reconstructed strike point position is well aligned with the peak of the emission, and the time response to changes in target location is very good, especially at larger strike point radii (>0.9m). There is some overshoot at smaller radii, likely indicating that the plasma response to the divertor coils changes appreciably over the range of radii considered. This motivates future research into upgrading the algorithm to automatically update the M matrix and PID gains in response to changes in the X-point and strike point targets.

4.4. Control of δr_{sep}

Control of the parameter δr_{sep}, defined as the distance between the radial position of the two points on the outer mid-plane that have the same flux as the upper and lower X-points, has also been commissioned and used to produce double null, as well as lower-, and upper-biased single null discharges. A series of equilibria showing a feedback controlled scan of δr_{sep} is shown in Figure 12. Time traces comparing the target and achieved δr_{sep} during these shots are shown in Figure 13. The δr_{sep} control method has been updated from that used on NSTX to adjust the boundary control point targets in real-time based on the measured δr_{sep} tracking error in order to appropriately bias the target shape to track the requested δr_{sep}. The value of δr_{sep} is calculated in real-time as

$$\delta r_{sep} = \left(\psi_{x,1} - \psi_{x,1}\right)/G_{mp}, \tag{8}$$

where G_{mp} is the radial flux gradient at the outboard mid-plane control point. The tracking error $\delta r_{sep} - \delta r_{sep,req}$ is then operated on with a PID controller to produce the

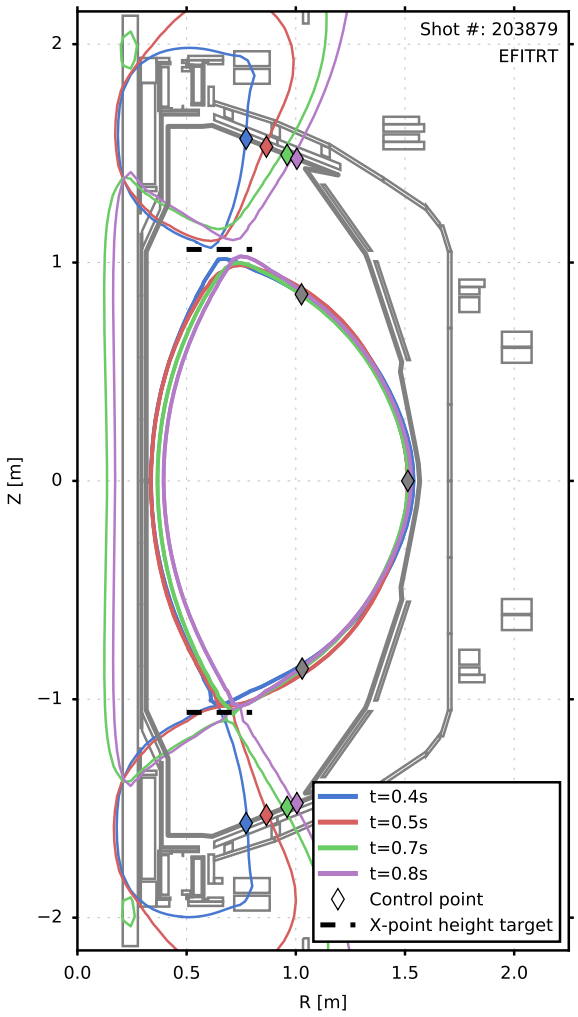

Figure 10. Plasma boundary at various times 203879 showing tracking of the strike point targets (colored diamonds on outboard divertor) while maintaining the outer gap targets (red diamonds) and the height of the X-points (dashed black lines).

value P_{sym}, which is used to calculate an adjustment a_i of the control point for the i-th control segment (in meters, along the control segment) as

$$a_i = (G_{mp}/G_i)\left(s_t \delta r_{sep,req} f_i + s_{PID} K_i P_{sym}\right), \tag{9}$$

where G_i is the flux gradient along the i-th control segment at the i-th control point, K_i is a feedback gain for the i-th control segment, f_i is the feedforward gain for the i-th control segment. The terms s_t and s_{PID} are signs and weights that change depending on the sign of δr_{sep}: for lower biased shapes, only the segments in the upper half of the device are adjusted with a weight of 1, for upper biased shaped, only the segments in the lower half of the device are adjusted with a weight of 1, and for balanced shapes, all segments are adjusted with the weight reduced to 0.5. This is in contrast to the older method in which the target shape was biased by a feedforward adjustment and the δr_{sep} tracking error was used to augment the PF3 voltage request. The older method resulted

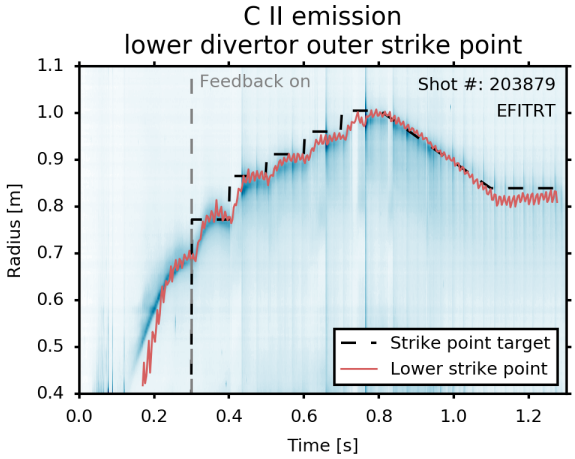

Figure 11. Carbon II emission on the lower divertor during shot 203879 overlayed with the target strike point location (black, dashed), showing that the EFITRT estimated strike point position (red, solid) is well aligned with the peak of the emission and tracks the target after feedback is turned on.

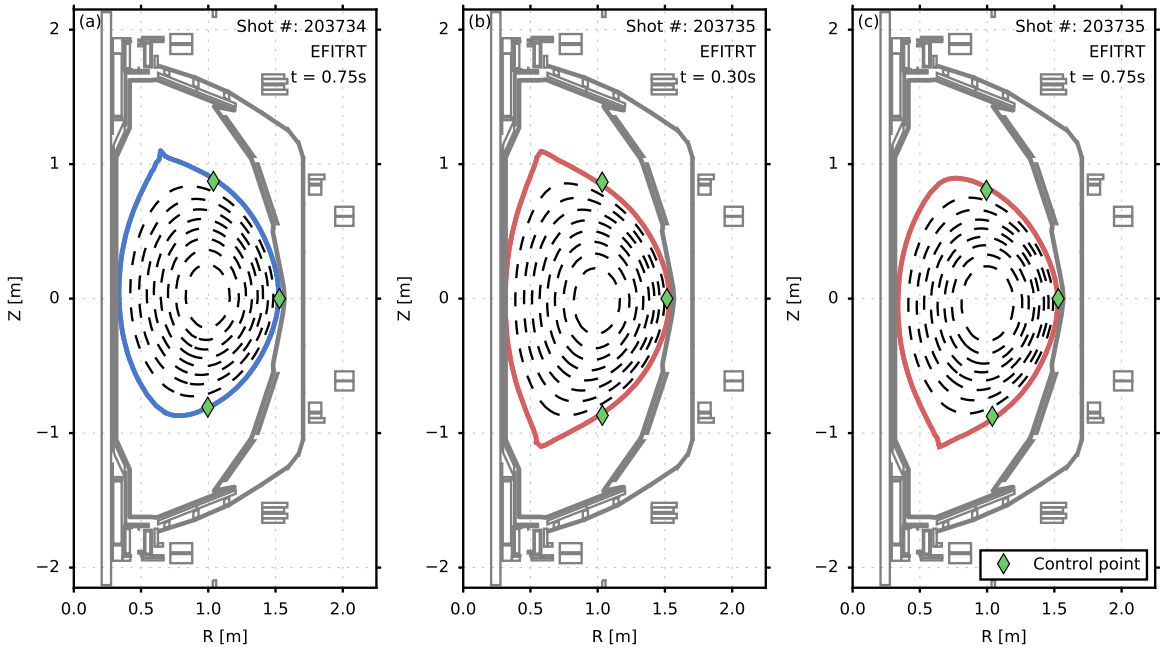

Figure 12. A series of three equilibria (a) 203734, t=0.75s, (b) 203735, t=0.3s, (c) 203735, t=0.75s, from two discharges in which the target for δr_{sep} was ramped from 0 cm to ±1 cm during the discharge. The target boundary locations are shown as red diamonds.

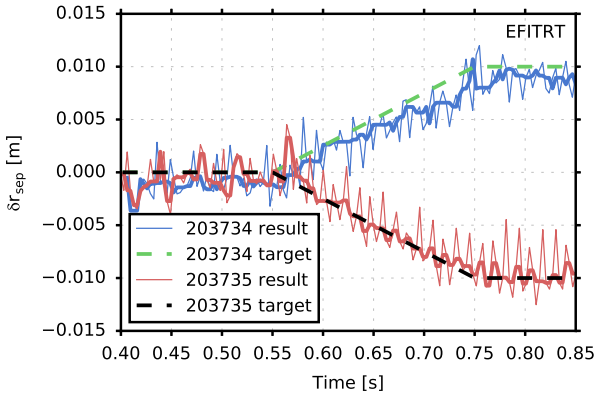

Figure 13. Comparison of the achieved (solid) and target (dashed) δr_{sep} in shots 203734 (blue) and 203735 (red). The thicker solid lines are the achieved values with a 5 sample median filter applied to remove the oscillations in the reconstruction caused by aliasing of divertor coil current ripple (these shots preceded the introduction of the anti-aliasing filters described in Section 3).

in inconsistencies between the target shape and the shape needed to achieve δr_{sep} target that made feedback loop tuning and interpretation of results more complex.

4.5. Control of mid-plane inner gap size

A new method for controlling the inner gap (the mid-plane gap between the plasma boundary and the center-stack) has also been commissioned for NSTX-U. Inner gap control on a spherical torus is challenging because there are no coils on the in-board side of the machine. Furthermore, each of the active shaping coils currently in use on NSTX-U have been assigned to controlling points on the outboard side of the machine, or to controlling the X-point or strike-positions, meaning the inner gap cannot be independently controlled. In the approach taken, the target locations of each control point along with the X-point radial and vertical target locations are modified away from the pre-programmed values in real-time to achieve the inner gap target. The flux error at the target location of the mid-plane inner plasma boundary is operated on by a PID operator to form P_{inner}. This flux error is then used to calculate an adjustment to the i-th control point $a_{inner,i}$ based on a weight for the i-th control point H_i, i.e.,

$$a_{inner,i} = P_{inner} H_i / G_{inner}, \tag{10}$$

where G_{inner} is the radial flux gradient at the inner gap target location, which is used to convert the flux error to a positional error. This scheme, illustrated in Figure 14, allows the operator to easily chose from shot to shot how the plasma shape should change in real-time to track the inner gap target without having to modify the control gains for outer gap and X-point control. Figure 15(a) compares the achieved and requested inner gap in shot 204742, in which the requested inner gap was ramped from around 3cm to 7cm between 0.7s and 0.9s. Because the integral gain was small in this example, a steady state error persists throughout the shot, however, it is clear that the controller is

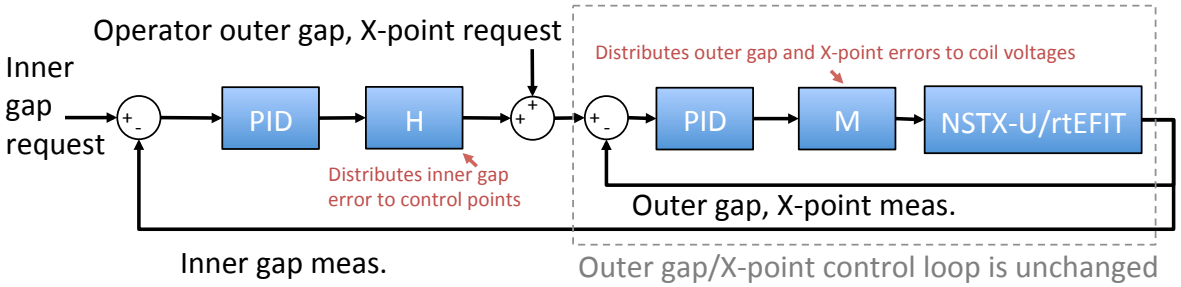

Figure 14. Schematic of isoflux modifications to isoflux shape controller for inner gap control showing how the outer gap and X-point requests are adjusted based on the inner gap error.

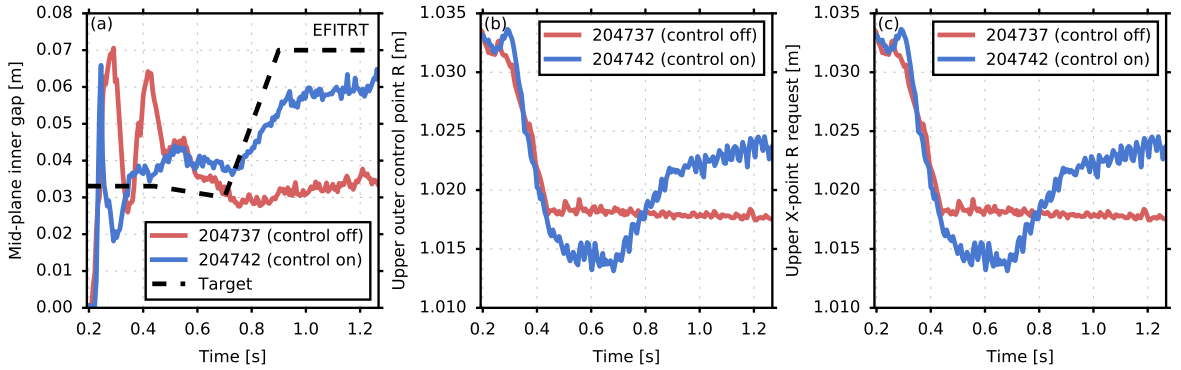

Figure 15. (a) Achieved (blue) and target (red, dashed) inner gap in discharge 204742. X-point radial target (b) and radial position of the upper-outer-squareness control point (c) showing the feedback modified targets in 204742 compared to those with inner gap control off in 204737.

able to modify the gap with good time response. The modification of the target X-point radial position and the radial position of the control point on the upper outer control segment is shown in Figure 15(b) and (c), respectively. The corresponding values in the reference shot 204737, which did not have inner gap control activated, are shown for comparison. The X-point and control point locations are moved slightly inboard to decrease the inner gap, then ramped to larger radii to increase the outer gap, with small modifications on the order of the requested change in inner gap.

5. Conclusion

Rapid progress has been made in commissioning the upgrades to the NSTX-U Plasma Control System, including the important areas of real-time reconstruction and boundary shape control. The resolution of real-time equilibrium reconstructions has been improved from what was used in NSTX to match that of the offline reconstruction code, fitting of the coil and vessel currents in real-time has been activated, and measurement filtering has been added to improve reconstruction quality. The plasma shape control algorithms have been updated and tuned for the new device, enabling accurate reproducible control

of the plasma boundary locations during all phases of the discharge. A flux projection gap control algorithm has been established for early in the discharge as well as during the ramp-down phases of the discharge, enabling outer gap and elongation control when real-time reconstructions are unreliable. During the remainder of discharges, real-time reconstructions are used to produce flux and position errors for the ISOFLUX control scheme to respond to. ISOFLUX control of the boundary locations and δr_{sep} has been demonstrated, and the ability to automatically switch the reference flux used in determining flux errors when the plasma transitions from limited to diverted configurations has been added. This new capability improves boundary control near the time of diverting. MIMO control of the X-point and strike point locations was demonstrated, and a new MIMO approach to controlling the mid-plane inner gap in real-time, a challenge for spherical torus devices, has been implemented and tested. These tools have been critical to the early commissioning activities on NSTX-U, especially for the development of L-mode and H-mode scenarios, and will be used to enable careful scans of shaping parameters during future campaigns.

Next steps for real-time reconstruction on NSTX-U will involve adding motional Stark effect (MSE) and Thomson scattering constraints, which will improve the estimation of internal profiles, and working to improve parallelization of the reconstruction algorithm to enable multiple iterations. Next steps for real-time control include commissioning feedback control algorithms for the plasma stored energy, current profile, rotation profile, and the 'snowflake' divertor configuration. The use of a fully multi-input multi-output control scheme that accounts for the interaction of the coils on all controlled quantities will also be explored [44].

Acknowledgements

This work was supported by the US Department of Energy Grant under contract number DE-AC02-09CH11466.

References

[1] MENARD, J., GERHARDT, S., BELL, M., et al., Nuclear Fusion **52** (2012) 083015.
[2] MENARD, J. E., ALLAIN, J. P., BATTAGLIA, D. J., et al., Nuclear Fusion **57** (2017) 102006.
[3] BATTAGLIA, D. J. et al., Nuclear Fusion, to be submitted (2017).
[4] GUTTENFELDER, W. et al., Nuclear Fusion, to be submitted (2017).
[5] ONO, M., KAYE, S., PENG, Y.-K., et al., Nuclear Fusion **40** (2000) 557.
[6] SYKES, A., AKERS, R., APPEL, L., et al., Nuclear Fusion **41** (2001) 1423.
[7] GOLDSTON, R., MENARD, J., ALLAIN, J., et al., An Experiment to Tame the Plasma Material Interface FT/P3-12, in *Proc. 22nd Int. Conf. on Fusion Energy*, Geneva, Switzerland, 2008, IAEA.
[8] STAMBAUGH, R. D., CHAN, V. S., WONG, C. P. C., et al., Candidates for a Fusion Nuclear Science Facility (FDF and ST-CTF) P2.110, in *37th EPS Conf. on Plasma Physics*, volume 51, Dublin, Ireland, 2010.
[9] MENARD, J. E., BROWN, T., EL-GUEBALY, L., et al., Nuclear Fusion **56** (2016) 106023.
[10] MENARD, J., BROMBERG, L., BROWN, T., et al., Nuclear Fusion **51** (2011) 103014.

[11] KAYE, S., ABRAMS, T., AHN, J.-W., et al., Nuclear Fusion **55** (2015) 104002.
[12] KAYE, S., BELL, M., BELL, R., et al., Nuclear Fusion **46** (2006) 848.
[13] KAYE, S., BELL, R., GATES, D., et al., Physical Review Letters **98** (2007) 175002.
[14] KAYE, S., LEVINTON, F., STUTMAN, D., et al., Nuclear Fusion **47** (2007) 499.
[15] VALOVIC, M., AKERS, R., DE BOCK, M., et al., Nuclear Fusion **51** (2011) 073045.
[16] FREDRICKSON, E. D., BELL, R. E., DARROW, D. S., et al., Physics of Plasmas **13** (2006) 056109.
[17] GRYAZNEVICH, M., SHARAPOV, S., LILLEY, M., et al., Nuclear Fusion **48** (2008) 084003.
[18] PODESTA, M., HEIDBRINK, W. W., LIU, D., et al., Physics of Plasmas **16** (2009) 056104.
[19] FREDRICKSON, E. D., CROCKER, N. A., BELL, R. E., et al., Physics of Plasmas **16** (2009) 122505.
[20] GATES, D., MENARD, J., MAINGI, R., et al., Nuclear Fusion **47** (2007) 1376.
[21] MENARD, J., BELL, M., BELL, R., et al., Nuclear Fusion **47** (2007) S645.
[22] GATES, D., AHN, J., ALLAIN, J., et al., Nuclear Fusion **49** (2009) 104016.
[23] GERHARDT, S., GATES, D., KAYE, S., et al., Nuclear Fusion **51** (2011) 073031.
[24] BUTTERY, R., AKERS, R., ARENDS, E., et al., Nuclear Fusion **44** (2004) 1027.
[25] CHAPMAN, I., COOPER, W., GRAVES, J., et al., Nuclear Fusion **51** (2011) 073040.
[26] FERRON, J. R., PENAFLOR, B., WALKER, M. L., MOLLER, J., and BUTNER, D., A flexible software architecture for tokamak discharge control systems, in *Proceedings of 16th International Symposium on Fusion Engineering*, volume 2, pp. 870–873 vol.2, 1995.
[27] PENAFLOR, B. G., FERRON, J. R., HYATT, A. W., et al., Latest advancements in diii-d plasma control software and hardware, in *2013 IEEE 25th Symposium on Fusion Engineering (SOFE)*, pp. 1–4, 2013.
[28] ERICKSON, K., GATES, D., GERHARDT, S., et al., Fusion Engineering and Design **89** (2014) 853.
[29] BOYER, M., ANDRE, R., GATES, D., et al., Nuclear Fusion **57** (2017) 066017.
[30] GOUMIRI, I. R., ROWLEY, C. W., SABBAGH, S. A., et al., Physics of Plasmas **24** (2017) 056101.
[31] GOUMIRI, I., ROWLEY, C., SABBAGH, S., et al., Nuclear Fusion **56** (2016) 036023.
[32] BOYER, M., ANDRE, R., GATES, D., et al., Nuclear Fusion **55** (2015) 053033.
[33] GATES, D., FERRON, J., BELL, M., et al., Nuclear Fusion **46** (2006) 17.
[34] GERHARDT, S., KOLEMEN, E., LAWSON, J., et al., Fusion Science and Technology **61** (2010) 11.
[35] KOLEMEN, E., GATES, D., ROWLEY, C., et al., Nuclear Fusion **50** (2010) 105010.
[36] KOLEMEN, E., GATES, D., GERHARDT, S., et al., Nuclear Fusion **51** (2011) 113024.
[37] BERKERY, J. W., SABBAGH, S. A., BELL, R. E., GERHARDT, S. P., and LEBLANC, B. P., Physics of Plasmas **24** (2017) 056103.
[38] FERRON, J., WALKER, M., LAO, L., et al., Nuclear fusion **38** (1998) 1055.
[39] GERHARDT, S. P., ERICKSON, K., KAITA, R., et al., Review of Scientific Instruments **85** (2014) 2012.
[40] GATES, D. A., MENARD, J. E., and MARSALA, R. J., Review of Scientific Instruments **75** (2004) 5090.
[41] SABBAGH, S., SONTAG, A., BIALEK, J., et al., Nuclear Fusion **46** (2006) 635.
[42] SABBAGH, S., KAYE, S., MENARD, J., et al., Nuclear Fusion **41** (2001) 1601.
[43] HOFMANN, F., Nuclear Fusion **30** (1990) 2013.
[44] SHI, W., BARTON, J., ALSARHEED, M., and SCHUSTER, E., Multivariable multi-model-based magnetic control system for the current ramp-up phase in the national spherical torus experiment (NSTX), in *50th IEEE Conference on Decision and Control and European Control Conference*, pp. 235–254, Orlando, FL, USA, 2011, IEEE.